Optimal implementation of a microspectrometer based on a single flat diffraction grating

Semen Grabarnik,[1,*] Arvin Emadi,[1] Elena Sokolova,[2] Gleb Vdovin,[1] and Reinoud F. Wolffenbuttel[1]

[1]Faculty Electrical Engineering, Mathematics and Computer Science, Department of MicroElectronics/Electronic Instrumentation, Delft University of Technology, Mekelweg 4, 2628 CD, Delft, The Netherlands

[2]River Diagnostics B.V., Dr. Molewaterplein 50, EE 1979, 3015 GE Rotterdam, The Netherlands

*Corresponding author: s.grabarnik@tudelft.nl

Received 19 December 2007; revised 18 March 2008; accepted 21 March 2008; posted 24 March 2008 (Doc. ID 91015); published 16 April 2008

An analytical model has been developed and applied to explore the limits in the design of a highly miniaturized planar optical microspectrometer based on an imaging diffraction grating. This design tool has been validated as providing the smallest possible dimensions while maintaining acceptable spectral resolution. The resulting planar spectrometer is composed of two parallel glass plates, which contain all components of the device, including a reflective slit and an imaging diffraction grating. Fabrication is based on microelectromechanical system technology and starts with a single glass wafer; IC-compatible deposition and lithography are applied to realize the parts in aluminum, which makes the microspectrometer highly tolerant for component mismatch. The fabricated spectrometer was mounted directly on top of an image sensor and takes up a volume of only 50 mm^3. The measured spectral resolution of 6 nm (FWHM) in the 100 nm operating wavelength range (600–700 nm) is in agreement with a model calculation.

OCIS codes: 300.6190, 220.2740, 050.1950, 230.3990.

1. Introduction

Optical microspectrometers fabricated using microelectromechanical system (MEMS) technology in silicon have a huge potential in applications where either extreme requirements on size or weight (such as space), or low costs per unit in high volume with a user-friendly interface (such as point-of-care medical diagnostics) are decisive. The benefits of a miniaturized system and the cointegration with microelectronic circuits are generally at the expense of moderate optical specifications [1]. Microspectrometers based on optical resonance (mostly Fabry–Perot) and on diffraction gratings have been demonstrated. Although resonator-based devices have found application in channel separation for optical communication, grating-based MEMS systems have proven more suitable for operation over a wide spectral range [1]. To date, only lensless MEMS-based systems with a simple transmission grating that yield limited resolution have been realized due to the technological constraints of IC-compatible processing [2,3].

The resolving power of a grating-based spectrometer, when using the first-order diffraction spectrum, is in principle equal to the number of grooves N in the grating, $R = N$. However, this assumes Fraunhofer diffraction with the distance between the grating (which can, within this context, also be considered a single slit) and the surface onto which the dispersed spectrum is projected (i.e., the detector array) larger than the Rayleigh distance $D = w^2/\lambda$, where w denotes the slit width and λ the wavelength of the light incident on the slit. In the case of an N element grating with a pitch p (a regular pattern of $p/2$ wide aluminum strips spaced at $p/2$), the slit width is $w = N \times p$. The resulting Rayleigh distance at wavelength λ is equal

0003-6935/08/122082-09$15.00/0

to: $D = N^2p^2/\lambda \sim 1\,\mathrm{cm}$. Such a dimension is poorly compatible with MEMS technology. Hence, Fresnel diffraction describes the optical behavior more adequately in a practical lensless MEMS-based system and limits the achievable resolving power to $R_{\max} = \lambda/\Delta\lambda \sim 20$ [1].

The most effective approach to circumvent this limitation is to design a microspectrometer based on an aspherical concave diffraction grating. However, such a device is difficult to combine with planar IC technology. A compromise lies in a flat imaging diffraction grating, which is presented in this paper. Because of the imaging properties of such a grating it is possible to combine collimating, dispersion, and focusing in a single optical element, thus simplifying the spectrometer design considerably.

Imaging gratings are relatively easy to implement in waveguide-based systems and compact spectrometers have been described in the literature [4–8]. Classical spectrometers with planar diffraction gratings have also been demonstrated [9]. These microspectrometers have a volume typically in the $1\,\mathrm{cm}^3$ range with a 5 nm resolution within a 100 nm spectral range. A promising result was obtained by employing integrated optics for the realization of a spectrometer with the largest dimension of $\sim$1.2 cm and a spectral resolution varying from 0.3 to 4.6 nm in the 150 nm wavelength range [7]. In [8] the authors expect for a waveguide spectrometer a theoretically feasible resolution of 2 nm within a 300 nm operating bandwidth based on numerical simulations. Several flat diffraction gratings can be combined to improve the imaging properties of an optical system [10]. Such an approach applied to a spectrometer can result in an increased spectral resolution [11,12].

The objective of this work is threefold: first, to provide a generalized analytical model that is able to tackle the problems of the miniaturization of a spectrometer and to determine the physical limits of the performance characteristics as a function of the critical dimensions, while using a single imaging diffraction grating and complying with constraints imposed by IC technology; second, to actually apply this model in the design of such a microspectrometer with a volume at least 1 order of magnitude smaller than so far reported in the literature; and third, to fabricate this microspectrometer in MEMS technology using a design that also addresses the alignment problem.

An analysis of the imaging properties of a single-wavelength optical system employing diffraction optical elements has been presented, for example, in the articles [10,13]. The goals and parameters considered in the design of a single-wavelength system are different from the optimization targets and design parameters related to a miniaturized spectrometer. That is why the analysis and conclusions in [10,13] are not applicable directly to the design of a microspectrometer. In this article, such an analysis was modified and combined with the diffraction grating theory and then applied to the problem of the optimal design of a microspectrometer [14,15]. As a result, an analytical model of a spectrometer has been developed. It takes into account such factors as optical aberrations and diffraction effects, which do significantly influence the spectral resolution of a spectrometer when scaling down the characteristic dimension to the millimeter range. The model covers a number of generic spectrometer designs based on a planar imaging diffraction grating and, with minor modifications, it is also applicable in the design of waveguide spectrometers based on focusing grating couplers. The model allows the estimation of the best achievable spectral resolution of a spectrometer at its main design parameters, minimizing the dimensions of the device.

The fabrication concept builds on the understanding that the optical performance critically depends on the alignment of the components in the microspectrometer system. As a consequence, the planar spectrometer design is composed of two parallel glass plates and mounted directly on the surface of an imaging sensor. All spectrograph components, including the input slit and the diffraction grating, are fabricated on one plane wafer. Thus, the slit and the grating are automatically aligned. Fabrication starts with a single glass wafer and IC-compatible deposition and lithography are applied to realize the parts in aluminum. The design allows relaxed alignment tolerances of the two glass plates after dicing: 15 μm for the spacing and 100 μm lateral misalignment of the glass plates, which highly simplifies assembly of the device. The fabricated device was mounted directly on top of an image sensor, takes a volume of only $1.5 \times 3 \times 11 = 50\,\mathrm{mm}^3$ and features a 6 nm spectral resolution in a 100 nm operating range of 600–700 nm.

2. Theoretical Considerations of an Imaging Grating-Based Spectrometer

The resolution of a spectrometer can be calculated as a product of the diffraction grating dispersion and the spot size produced by the imaging system when the entrance slit is illuminated with a monochromatic light. Following the analysis of a single-wavelength imaging system in [10,13], the spot size can be estimated as a sum of different contributions, including diffraction broadening and aberrations. In the case of a spectrometer, the width of the image of the entrance slit should also be considered. The calculation of the dispersion, the diffraction broadening, and the entrance slit image is straightforward. To take the aberrations into account the geometrical theory of the diffraction gratings [14,15] can be used. Figure 1(a) presents the geometry of a diffraction grating that images point A into point B. Plane yz of the coordinate system $oxyz$ lies in the grating plane and the origin of the coordinate system, o, coincides with the grating central point O. Consider point O and a point $P(y,z)$ somewhere in the grating plain.

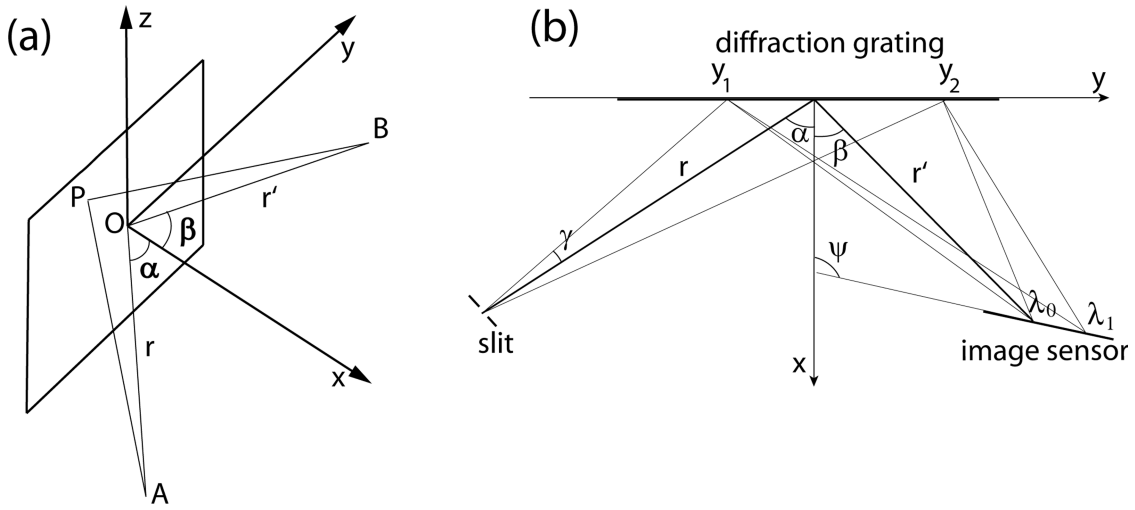

Fig. 1. (a) Schematic of a diffraction grating imaging point A in to point B and (b) principal design of an imaging grating-based spectrometer.

Then the optical path difference between light beams passing from A `to B via point P and via point O is

$$F(\lambda, y, z) = APB - AOB + m\lambda N(y, z), \qquad (1)$$

where $N(y,z)$ is the number of grooves between points O and $P(y,z)$, m is a diffraction order, and λ is a wavelength. The function in Eq. (1) can be decomposed into power series and take the form

$$F(\lambda, y, z) = \sum_{i=0}^{\infty}\sum_{j=0}^{\infty} F_{ij} y^i z^j = \sum_{i=o}^{\infty}\sum_{j=0}^{\infty} (M_{ij} + m\lambda N_{ij}) y^i z^j. \qquad (2)$$

A path difference F in Eq. (2) equal to zero corresponds to the aberration-free convergent wavefront. Thus, the coefficients F_{ij} define deviations of the wavefront proportional to $y^i z^j$ and can be considered as the aberration coefficients. The coefficients M_{ij} depend on the system configuration and the coefficients N_{ij} are determined by the grating groove pattern [15]. For the wavelength λ_0 the coefficients N_{ij} can be selected in such a way that the aberration coefficients F_{ij} are zero, thus yielding an aberration-minimum image of a point A. Given the geometrical parameters of the system, the grating coefficients can be calculated analytically:

$$N_{ij} = -\frac{M_{ij}}{m\lambda_0} = \frac{1}{i!j!m\lambda_0}\left[\frac{\partial^{i+j}(APB - AOB)}{\partial y^i \partial z^j}\right]_{(0,0)}. \qquad (3)$$

Exact formulae for N_{ij} are listed in, for example, [15]. The groove pattern defined by the coefficients N_{ij} resembles a part of a diffraction lens, since it takes the shape of a set of curved grooves not equally distributed in the grating plane. The local period of such a grating along the oy axis is $d = (\partial N/\partial y)^{-1}$. The period d at the central grating point is referred to as the grating period d_0. The parameter λ_0 in Eq. (3) is the design wavelength, which is the central wavelength of the spectrometer operating bandwidth.

A schematic of a spectrograph setup is shown in Fig. 1(b). In the design optimization only the xoy plane is considered, since this is the dispersion plane of the grating. Incident light entering through the entrance slit is directed to the grating at the angle α, with the grating normal, and diffracts toward the photodetector array at the angle β relative to the normal. The parameters of the design are the incident angle α, input aperture angle γ, distance r from the input slit to the grating surface, grating period d_0, position of the image sensor plane (determined by the distance r' and angle ψ), and the design wavelength λ_0. The size of the illuminated part of the grating, $L = y_1 - y_2$, is defined by r, α, and γ and can be calculated from the simple geometrical considerations, as shown in Fig. 1(b). At any set of design parameters the resolution of such a spectrometer can be determined considering the contributions of the relevant factors: optical aberrations, diffraction broadening of the image, and influence of the slit width.

An imaging diffraction grating designed using Eq. (3) to calculate the grating coefficients reduces aberrations at the design wavelength λ_0. However, for the wavelengths not equal to λ_0, the optical path difference (Eq. (2)) is no longer zero and the image of the slit in the detector plane is broadened. This angular broadening can be calculated from the geometrical considerations using the equation for transverse ray aberrations [16]:

$$s_{\text{aberr}} = \left.\frac{\partial F}{\partial y}\right|_{y=y_1} + \left.\frac{\partial F}{\partial y}\right|_{y=y_2}. \qquad (4)$$

For a finite number of the row members in Eq. (2) the value of s_{aberr} can be calculated analytically using Eqs. (2)–(4). Note that the coefficients N_{ij} in Eq. (2)

are calculated only once for the design wavelength, while the coefficients M_{ij} should be recalculated for another value of the wavelength taking into account that values of β and r' change with the wavelength.

The spatially finite size of the illuminated part of the grating leads to the diffraction broadening of the image of a point source. Such a broadening can be estimated as follows:

$$s_{\mathrm{diffr}} = \frac{2\lambda}{y_2 - y_1}. \tag{5}$$

The width of the entrance slit also influences the spectral resolution since the smaller the entrance slit, the smaller its image on a photodetector. However, there is an optimal slit width defined by the input aperture and reducing the entrance slit further would not improve the resolution. The angular width of the entrance slit image is:

$$s_{\mathrm{slit}} = \frac{\cos(\alpha)}{\cos(\beta)} \times \frac{s_0}{r}, \tag{6}$$

where $s_0 = \lambda/\gamma$ is the optimal width of the entrance slit.

The resolution of the spectrometer $\Delta\lambda$ can be found as the product of the angular dispersion and the sum of different contributions given by the Eqs. (4)–(6):

$$\begin{aligned}\Delta\lambda &= \Delta\lambda(\lambda, \lambda_0, \alpha, r, \beta, r', \gamma, \psi) \\ &= f \times (s_{\mathrm{slit}} + s_{\mathrm{aberr}} + s_{\mathrm{diffr}}).\end{aligned} \tag{7}$$

The angular dispersion of the grating is defined by

$$f = d_0 \times \cos(\beta). \tag{8}$$

Equations (1)–(8) are the basis of the model describing the dependence of the spectrometer resolution on different parameters. It should be emphasized that these equations (except for Eq. (5)) result from a geometrical optics approach and provide an estimate of the resolution based on the calculation of the entrance slit image width, multiplied by the dispersion. However, geometrical optics cannot provide precise values of the resolution, since a diffraction analysis should be used that takes into account the phase and interference of the light. An accurate resolution estimate can be obtained via calculation of the point spread function (PSF) of the imaging system, convoluted with the transmission function of the entrance slit. The width of this curve measured at half-maximum level and multiplied by the dispersion gives an accurate value for the resolution. For a spectrometer with optical aberrations that are small compared to the diffraction-limited performance of the system, the estimation of resolution based on the geometrical optics would give an overestimated value, as opposed to the value obtained by diffraction analysis. Equation (5) was included in the model to compensate for such a discrepancy. In the case of a system with relatively large optical aberrations, which is typically the case in a microspectrometer, the geometrical approach would provide an underestimated result. In this case, Eqs. (1)–(8) provide an estimate of the resolution defined as a full width of a monochromatic spectral line at zero level, which implies that the resolution of an actual spectrometer defined as the width of the monochromatic line at half-maximum is approximately 2× higher than the one predicted by the model. Therefore, this factor of 2 is included in the resolution specifications in terms of FWHM that result from the analytical modeling discussed in this paper.

The model based on Eqs. (1)–(8) can also be applied for a waveguide spectrometer based on a focusing grating coupler with the following modifications: incidence angle is fixed and equal to $\pi/2$ and the width of the grating L is an input parameter for the model. The distance from the grating coupler to the detector plane is thus considered the largest dimension of a waveguide spectrometer. The advantage of such a spectrometer is that, for a single mode waveguide, the contribution of the entrance slit width is zero, since there exists only one mode propagating parallel to the waveguide surface. Thus the resolution of the waveguide spectrometer is

$$\Delta\lambda_{wg} = f \times (s_{\mathrm{aberr}} + s_{\mathrm{diffr}}), \tag{9}$$

where f, s_{aber}, and s_{diff} are defined by Eqs. (4), (5), and (8).

3. Analysis of the Model

Some of the parameters in Eq. (7) should be set to values dictated by technological constraints or design targets. Hence, these are fixed in order to study the dependence of the resolution on the other parameters. Figure 2 shows the dependence of the resolution on the incident angle α and the input aperture angle γ within the operating bandwidth of 100 nm. The fixed parameters in Eq. (7) are due to design

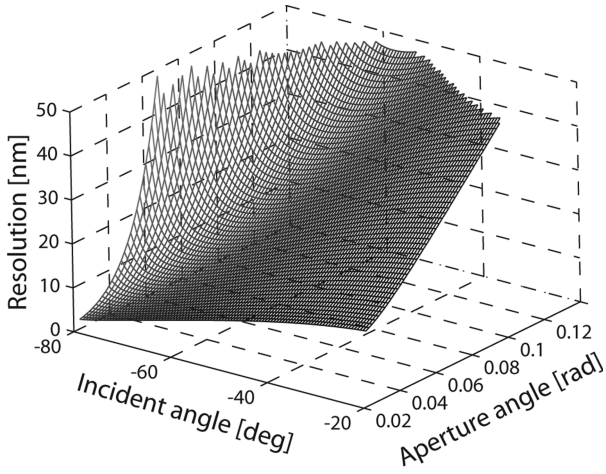

Fig. 2. Dependence of spectral resolution on angle of incidence and input aperture.

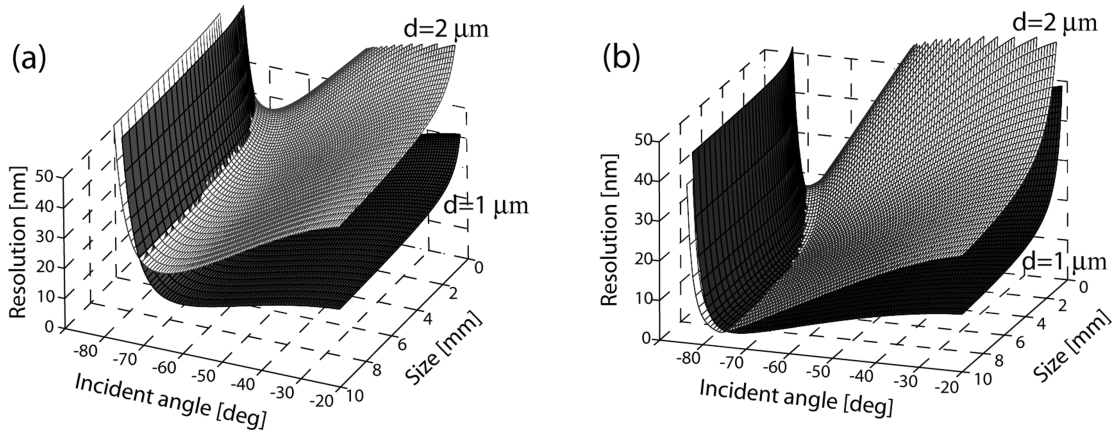

Fig. 3. Dependence of the resolution within a 100 nm bandwidth on the angle of incidence and size (the distance from the entrance slit to the grating) of a spectrometer. The results are for the grating period 1 μm and 2 μm with (a) input aperture 0.1 and (b) input aperture 0.05.

targets and are set at $r = r' = 10$ mm and $\lambda_0 = 650$ nm; those due to technological constraints are at $d_0 = 2\,\mu$m and $\psi = \pi/2$. From Fig. 2 it is evident that a small aperture angle and a large angle of incidence contribute to an improved resolution of the spectrometer. The improved spectral resolution with reduced aperture complies with intuition, since aberrations of the grating are the main contribution to the resolution function in Eq. (7). However, the input aperture angle also defines the optical throughput (or luminosity) of the spectrometer. The resulting signal reduction at the photodetector reduces the overall sensitivity of the device.

Since spectral resolution and throughput are not independent parameters it is necessary to fix the spectrometer input aperture angle to such a value that an acceptable signal-to-noise ratio results at the detector and to take the angle ψ as a variable. Also at this set of fixed parameters the dependence of the resolution within a specified wavelength range on the other design parameters, such as the incidence angle and distance from the slit to the grating r, can be investigated. Assume further that $r' = r$. Since r is the largest dimensional parameter in the design it is convenient to take it as a measure of the spectrometer size and in the following discussion r is referred to as the spectrometer size or dimension. The angle ψ between photodetector plane and the grating normal can be optimized to maximize resolution. It should be noted that the optimal value of the angle ψ does not depend on the spectrometer size. This statement is supported when considering the characteristics of a diffraction lens. The focal distance of such a lens is inversely proportional to wavelength. That is why the optimal value of ψ is defined by the angle of incidence and grating period. Since the angle at which light falls on the surface of a photodetector should not exceed some maximum value to avoid Fresnel reflection of a substantial part of radiation, this angle is limited in the model to 45°. Using Fig. 1 yields $\psi_{\max} = 180 - 45 - \beta$.

Figure 3 shows the spectrometer resolution depending on the angle of incidence and on spectrometer dimension. These dependencies were calculated for the operating range of 100 nm and two different values of the grating period. Results for the aperture angle of 0.1 and 0.05 rad are demonstrated in Figs. 3(a) and 3(b), respectively. For each data point in Fig. 3 the value of ψ was optimized. The optimal value gradually varies depending on the incidence angle from ~90° corresponding to the incidence angle of 20° to ~130° for an incidence angle of 80°. As can be derived from Fig. 3, the resolution is weakly dependent on the size of the spectrometer in cases where the size is larger than 5–4 mm. The best results are achieved at an angle of incidence in the 70°–75° range, irrespective of spectrometer size. The strong dependence of the resolution on angle of incidence is due to aberrations of the grating, which is the main contribution in the resolution dependence. The width of the entrance slit image and the diffraction broadening start to affect resolution for a spectrometer dimension smaller than 2–3 mm. This dependence is inversely proportional to r, which is in agreement with Eq. (6). For the optimal width of the entrance slit, the influence of the slit image and the influence of the diffraction broadening on the resolution are of the same order of magnitude. Figure 3 predicts a resolution of a plane grating spectrometer with dimension as small as 6 mm of ~5–10 nm within a 100 nm operating range provided that the input aperture angle of the spectrometer is sufficiently small (~0.05 rad). This result is the starting point in the microspectrometer design presented in Section 4.

4. Planar Spectrometer Design

The simplified structure of the planar imaging grating-based microspectrometer is shown in Fig. 4. The spectrometer consists of two pieces of glass aligned parallel to each other. All spectrometer optical components, including the input slit and the diffraction grating, operate in reflection. The light from a source

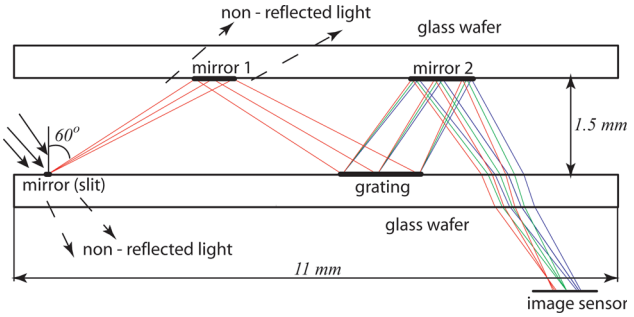

Fig. 4. (Color online) Design of the planar microspectrometer.

is reflected from a stripe mirror acting as a slit and then redirected by the upper mirror 1 to the diffraction grating. The diffracted light is reflected by mirror 2 and finally projected onto the photodetector (CCD imager) through the glass plate. Hence, the imaging system of the spectrometer projects the dispersed image of the reflective input slit onto the plane of the image sensor. In this sense the operation of the reflective slit is similar to the conventional slit in a classic spectrometer. The width of the slit mirror is 50 μm, which corresponds to the effective slit width of 25 μm when taking into account the 60° angle of incidence. The dimensions of mirror 1 define the input aperture of the spectrometer, since the nonreflected light escapes the system through the glass plate. As was already discussed in Section 3, the value of the angle of incidence in the range of 70°–75° would give a superior performance (Fig. 2); however, the amount of light reflected from the glass surfaces increases with incident angle due to Fresnel reflection. Such parasitic reflections contribute to the stray light, which is indeed observed in the fabricated device and is discussed in more detail in Section 5. Therefore, the design was based on an angle of incidence at 60°, as a compromise between stray light level and resolution.

The period of the grating d_0 (the local period in the grating center) should be minimized to achieve best resolution, as results from Fig. 3. For the lithographically fabricated grating the smallest period is constrained by the resolution of the available lithographic technology and is two times larger than the minimum feature size of the lithographic process. Taking into account that the local period varies along the grating and that the resolution of the available lithography was 0.7 μm, the parameter d_0 was chosen to be 2 μm. The input aperture angle was selected at 0.05 rad and the distance between the glass plates was 1.5 mm, which yields the very compact device shown in Fig. 4. The angle $\psi = 90°$ (see Fig. 1) is determined by the direct mounting of the image sensor in a planar structure. The optimal value according to the model, $\psi = 102°$, results in the improvement of the resolution by about 12%, as compared to the setup with $\psi = 90°$ (13 nm versus 14.6 nm, which is equivalent to 6.5 nm FWHM and 7.3 nm FWHM, respectively). The spectrometer design has been verified using rigorous ray tracing software ZEMAX [17]. The results of the model were in a good agreement with the resolution estimate based on geometrical ray tracing using ZEMAX. However, accurate calculation based on the PSF in ZEMAX resulted in a resolution of 5.6 nm FWHM. Hence, the analytical design provides a 30% underestimated result. In the final design step ZEMAX was used to estimate tolerances for the alignment of two spectrometer parts. The influence of the lateral misalignment and the errors in spacing between two glass plates on the spectral resolution were analyzed using the ZEMAX PSF cross section calculation. Any displacement of the glass plates results in a displacement of the mirrors (mirror 1 or 2 in Fig. 4) and thus in a change of the angle of incidence and the length of optical pass that light travels from the slit to the grating. Such an error is the reason for the aberrations of the grating not to be minimized at the design wavelength, but rather at a wavelength spectrally shifted from the designed value. Thus, a misalignment within reasonable bounds results in a small shift of the operating bandwidth. Having limited such a shift to 10 nm we obtained that the alignment tolerances are ~15 μm for the spacing and 100 μm for the lateral alignment of the glass plates. According to the ZEMAX PSF calculations the resolution is decreased by less than 10% within the shifted operating bandwidth.

Having the necessary design parameters defined, Eq. (3) can be used to calculate the grating coefficients. Subsequently, for each of the grating grooves a set of points (y,z) that is part of the groove and describe its position in the grating plane was determined. This procedure enabled generating the mask using IC design software tools. Figure 5 shows a part of the mask used for the lithographic fabrication of the grating. It features curved lines. The line spacing varies from 1.5 to 2.8 μm along the grating. Since the lithographic technique did not allow fabrication of blazed gratings, the only physical parameter available for optimization was the depth of the rectangular grating grooves, which was chosen to be equal to 230 nm, maximizing the diffraction efficiency for an Al-coated grating in the wavelength region from 600–700 nm. The resulting diffraction efficiency

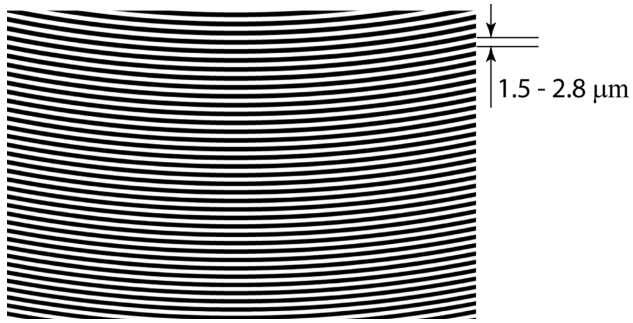

Fig. 5. Part of the mask used for the lithographic fabrication of the grating. The spacing between curved lines varied from 1.5 to 2.8 μm along the mask.

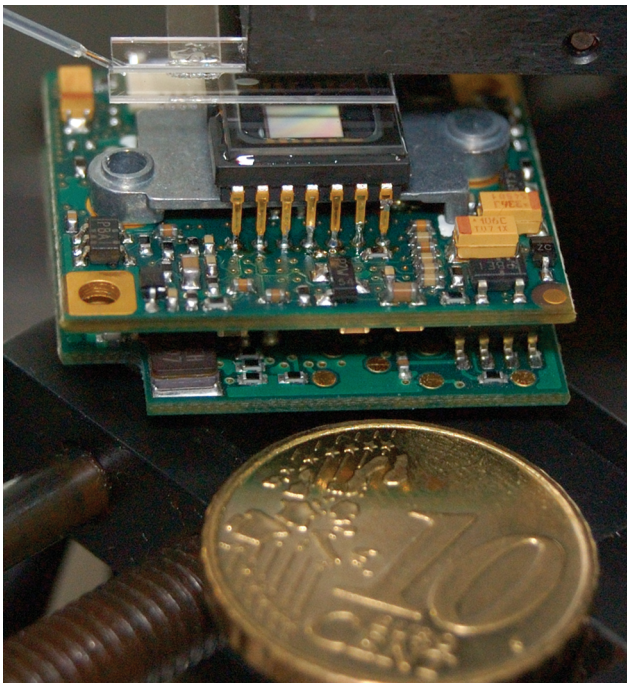

Fig. 6. (Color online) Experimental setup. The spectrometer is visible as two glass rectangles on top of the image sensor. The diffraction grating is visible as an ellipse on the lower rectangle. Light is fed into the spectrometer from the fiber tip shown in the upper left corner.

equals 38% at the wavelength of 630 nm and equals 29% at the wavelength of 680 nm. These values are low compared to the blazed gratings efficiency with the peak in the range of 70%–80%. A more complicated fabrication technology is required for increasing the efficiency of the grating used in a microspectrometer.

5. Fabrication and Characterization of the Spectrometer

All elements of the spectrometer, including the slit and the gratings, were fabricated on a single glass wafer with a two-mask lithography process. First, 650 nm of aluminum was deposited and the first mask was applied to define the grating structures. Subsequently, the gratings were plasma etched to yield 230 nm deep grooves in the aluminum. Finally, using the second mask, the aluminum was patterned and etched to define the input slit, the grating, and the mirrors. The grooves defined in the first step were protected during the etching. The processed wafer was diced and the two parts of the spectrometer were aligned and mounted on top of the CCD imaging sensor, as shown in Fig. 6. The measurements were carried out in a dark room to exclude light entering the system from the sides. A multimode optical fiber was used to feed the optical signal into the microspectrometer. One of the cleaved fiber tips was exposed to a light source under test and the second fiber tip illuminated the input slit of the spectrometer. As an example of the device's performance,

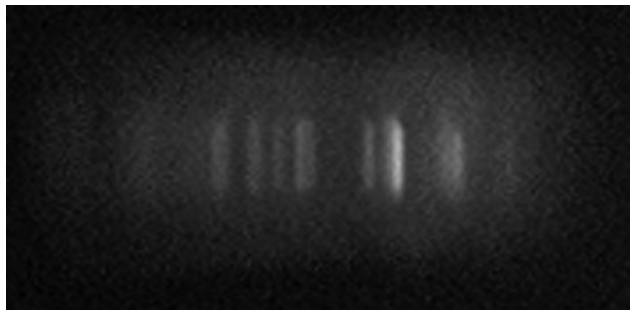

Fig. 7. Spectrum of a Ne lamp produced with the planar spectrometer and registered with the CCD image sensor.

Fig. 7 represents the spectrum of a Ne lamp captured with the device in the range between 630 and 730 nm.

The setup presented in Fig. 6 was equipped with several microscrews, which allow the adjustment of the position of the upper glass plate, while the position of the lower plate was fixed just above the image sensor. The optimal position of the upper plate was found experimentally by adjusting until the best spectral pattern with sharp lines was obtained. Moving the top glass plate up, down, left, and right from this optimal position within the tolerance bounds defined at the design stage did not result in an observable degradation of spectral resolution, since the visible spectral lines remained within the slightly shifted operating bandwidth.

The effect of stray light is clearly visible in Fig. 7. The Fresnel reflection of the glass surface around the input slit is, at the given angle of incidence (60°), about 9% of the light impinging on the input slit (see Fig. 4), whereas the reflectance of aluminum is about 90% in the visible spectral range [18]. Hence, the contrast is just a factor of 10. The spectral image presented in Fig. 7 is actually a superposition of the dispersed images of the entrance slit and the light spot of the fiber tip that was used for illumination of the slit. The elliptical images of the fiber tip can be recognized in Fig. 7. The elimination of Fresnel reflections would substantially decrease the level of stray light. It could be achieved by depositing an appropriate antireflection coating on the unused surfaces. The coating process would involve an additional lithography step: the deposition of an appropriate material on top of a wafer followed by the patterning of this material to open aluminum gratings and mirrors and that part of the glass plate that covers the image sensor. Implementation of such a coating is part of our future work.

The measured spectrum of Ne, as obtained with the microspectrometer, is shown in Fig. 8. The major lines are marked to identify them with the Ne spectral lines. From Fig. 8 we estimate the FWHM resolution to be ~6 nm, while the relative positions of spectral lines can be determined with a precision of better than 1 nm. Hence, the measured resolution of the spectrometer is 20% higher than the analytical

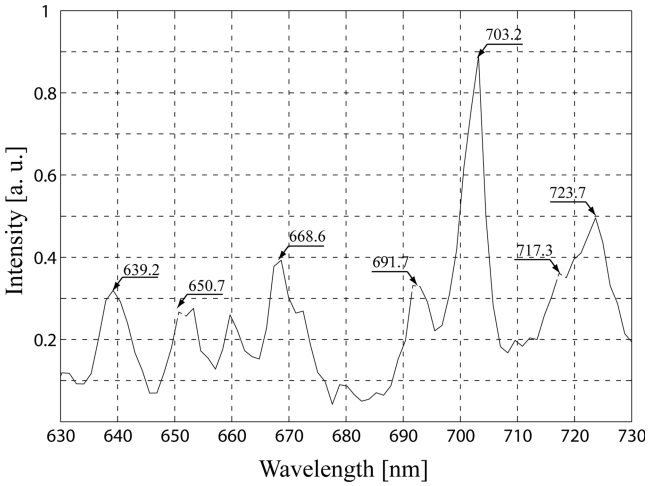

Fig. 8. Spectrum of a Ne lamp obtained with the microspectrometer.

predictions based on the geometrical approach presented in Fig. 3 and is in good agreement with the estimates obtained using the ZEMAX PSF calculation.

6. Conclusions

The first objective of this work was to generalize the problem of the miniaturization of a spectrometer employing a flat imaging diffraction grating on the basis of an analytical model. The simulations not only confirmed the reasonable expectation that optical aberrations are the major limiting factor to the spectral resolution of a miniaturized spectrometer, but also facilitated the design of the actual microspectrometer with dimensional constraints. The analysis of the model demonstrated that the best resolution of the spectrometer could be achieved with high incident angles (∼70°–75°) and a small input aperture angle (∼0.05 rad).

The second objective was to actually design a microspectrometer using the model to find optimal design parameters. Practical constraints led to a configuration that slightly departs from the model optimum. Fresnel reflections limited the incident angle to 60° and, due to the design planarity, the image sensor was parallel to the grating plane. With such constraints the FWHM resolution of the designed spectrometer was predicted to be ∼5.6 nm.

The third objective was the actual fabrication of the microspectrometer. The planar design simplifies its fabrication and assembly considerably. The highly miniaturized (dimensions only $11 \times 1.5 \times 3\,\mathrm{mm}^3$) spectrometer demonstrated a FWHM spectral resolution of 6 nm within a 100 nm operating range, which is in good agreement with the simulation results. The measured resolution of the spectrometer is 20% better than the analytical predictions based on the geometrical approach presented in Fig. 3 and is in good agreement with the estimates obtained using a ZEMAX PSF calculation. Although the PSF approach has been demonstrated to yield a more accurate result, the analytical approach based on geometrical optics presented here is more suitable for the interactive design of a microspectrometer with strict dimensional constraints.

Improvement of the resolution is possible if the design or technology constraints are relaxed. The most important constraint is the one for the incident angle resulting from the Fresnel reflection, as was discussed in Sections 4 and 5. If such reflections are eliminated using an antireflection coating the incident angle can be increased to the optimal value of about 76°, resulting in an improvement in spectral resolution by a factor of 3, which implies that a FWHM resolution below 2 nm is possible. A better spectrometer performance can also be achieved with a larger grating groove density. This would be possible with a higher resolution lithography process. The relaxed dimensional constraint cannot improve the resolution considerably, as shown in Fig. 3. For example, increasing the size of the device from 6 to 10 mm results in an improvement of the resolution of less than 10%. The last constraint is the numerical aperture, which is already small. However, for the applications involving very bright sources or sources with limited aperture this constraint can be mitigated.

Thus, future work will be directed toward the improvement of the planar spectrometer with respect to the elimination of Fresnel reflections at unused surfaces of the device and on the IC-compatible fabrication of more efficient diffraction gratings.

The authors acknowledge financial support from the Dutch Technical Foundation (STW), grant DET.6667. We are indebted to Lina Sarro and Charles de Boer (DIMES, TU Delft) for very useful discussions and wafer processing and to Jan Groeneweg and Jan Cornelis Wolff (DIMES, TU Delft) for the mask fabrication.

References

1. R. F. Wolffenbuttel, "MEMS-based optical mini- and microspectrometers for the visible and infrared spectral range," J. Micromech. Microeng. **15**, S145–S152 (2005).
2. T. A. Kwa and R. F. Wolffenbuttel, "Integrated grating/detector array fabricated in silicon using micromachining techniques," Sens. Actuators A, Phys. **31**, 259–266 (1992).
3. S.-H. Kong and R. F. Wolffenbuttel, "Spectral performance of a micromachined infrared spectrum analyzer in silicon," IEEE Trans. Instrum. Meas. **54**, 264–267 (2005).
4. H. W. Yen, H. R. Friedrich, R. J. Morrison, and G. L. Tangonan, "Planar Rowland spectrometer for fiber-optic wavelength demultiplexing," Opt. Lett. **6**, 639–641 (1981).
5. D. S. Goldman, P. L. White, and N. C. Anheier, "Miniaturized spectrometer employing planar waveguides and grating couplers for chemical analysis," Appl. Opt. **29**, 4583–4589 (1990).
6. D. Sander and J. Muller, "Selffocusing phase transmission grating for an integrated optical microspectrometer," Sens. Actuators A, Phys. **88**, 1–9 (2001).

7. K. Chaganti, I. Salakhutdinov, I. Avrutsky, and G. W. Auner, "A simple miniature optical spectrometer with a planar waveguide grating coupler in combination with a plano-convex lens," Opt. Express **14**, 4064–4072 (2006).
8. I. Avrutsky, K. Chaganti, I. Salakhutdinov, and G. Auner, "Concept of a miniature optical spectrometer using integrated optical and micro-optical components," Appl. Opt. **45**, 7811–7817 (2006).
9. S. Ura, F. Okayama, K. Shiroshita, K. Nishio, T. Sasaki, H. Nishihara, T. Yotsuya, M. Okano, and K. Satoh, "Planar reflection grating lens for compact spectroscopic imaging system," Appl. Opt. **42**, 175–180 (2003).
10. M. Testorf and J. Jahns, "Imaging properties of planar-integrated micro-optics," J. Opt. Soc. Am. **16**, 1175–1183 (1999).
11. S. Ura, T. Sasaki, and H. Nishihara, "Combination of grating lenses for color splitting and imaging," Appl. Opt. **40**, 5819–5824 (2001).
12. S. Grabarnik, R. Wolffenbuttel, A. Emadi, M. Loktev, E. Sokolova, and G. Vdovin, "Planar double-grating microspectrometer," Opt. Express **15**, 3581–3588 (2007).
13. R. K. Kostuk, J. W. Goodman, and L. Hesselink, "Design considerations for holographic optical interconnects," Appl. Opt. **26**, 3947–3953 (1987).
14. H. Noda, T. Namioka, and M. Seya, "Geometric theory of the grating," J. Opt. Soc. Am. **64**, 1031–1036 (1974).
15. C. Palmer and W. R. McKinney, "Imaging theory of plane-symmetric varied line-space grating systems," Opt. Eng. **33**, 820–829 (1994).
16. M. Born and E. Wolf, *Principles of Optics* (Cambridge, 2002).
17. ZEMAX optical design program user's guide, version 9.0 (Focus Software, 2000).
18. D. Rossberg, "Optical properties of the integrated infrared sensor," Sens. Actuators A, Phys. **54**, 793–797 (1996).